Restoration algorithm for noisy complex illumination

Zhanwen Liu[1,2], Tao Gao[1], Fanjie Kong[1], Ziheng Jiao[1], Aodong Yang[1], Shuying Li[3] ✉, Bo Liu[4]

[1]*School of Information Engineering, Chang'an University, Xi'an 710064, Shaanxi, People's Republic of China*
[2]*Institute of Transportation Studies, University of California, Berkeley, City of Berkeley, State of California CA 94804-4648, USA*
[3]*School of Automation, Xi'an University of Posts & Telecommunications, Xi'an 710121, Shaanxi, People's Republic of China*
[4]*Department of Computer Science and Software Engineering, Auburn University, Auburn, State of Alabama, AL 36849, USA*
✉ *E-mail: angle_lisy@163.com*

Abstract: Although promising results have been achieved in the restoration of complex illumination images with the Retinex algorithm, there are still some drawbacks in the processing of Retinex. Considering the noise characteristics of complex illumination images, in this study, we propose a novel restoration algorithm for noisy complex illumination, which combines guided adaptive multi-scale Retinex (GAMSR) and improvement BayesShrink threshold filtering (IBTF) based on double-density dual-tree complex wavelet transform (DDDTCWT) domain. Extensive restoration experiments are conducted on three typical types images and the same image with different noises. On the basis of a series of evaluation indexes, we compare our method to those of state-of-the-art algorithms. The results show that (i) SSIM of the proposed IBTF is superior to traditional Bayes threshold method by 15% as the standard variance is 100. (ii) PSNR of the proposed GAMSR enhances 15% to traditional MSR. (iii) The clarity of final results for restoration speeds up three times than that of original images, and the information entropy is improved slightly too. Therefore, the proposed method can effectively enhance the details, edges and textures of the image under complex illumination and noises.

1 Introduction

The digital image is referred to as one of the important sources of information. High-quality image under appropriate illumination is easy to process for information extraction. However, images captured in different conditions sometimes suffer from visibility degradation because the light is changing and the signal of the camera is interfered through unevenness media, such as fog, haze and noise. Fig. 1 shows five different images degraded by low brightness, low contrast and unevenness. It is obvious that complex illumination affects greatly on the quality of images. Developing an effective method to restore all the details of images collected in complex illumination is desirable.

Image restoration is always a fundamental problem in computer vision and has received increasing attention in the past few years [1]. Image restoration in complex illumination images with noise can improve the quality of these defective images, which not only provides rich details of the whole image [2, 3], but also extracts the local feature area [4, 5].

The mainstream technologies of image restoration on complex illumination images are based on the physical model [6] and tensile transformation [7, 8]. The former methods commonly establish a physical model considering the cause of fog formation, but it is difficult to make sure the accurate and effective of this model for various scenes. By devising and analysing properties transformation of the image, the latter aims at recovering the foggy images and fundamentally compensates for the loss of image details caused by complex illumination [9]. Moreover, the later mainly uses image histogram equalisation [10, 11], homomorphic filter [12–14], wavelet transform (WT) [15, 16] and Retinex transform [17, 18] for fog images or other low-quality images. However, there are too more thresholds and parameters to lead loss of information and lack of robustness for the method above. In this paper, we mainly focus on improvements to the latter mentioned methods.

The histogram equalisation method is to adjust the grey value of each pixel according to the rule of uniform distribution of probability, so as to improve the brightness and contrast of the image. However, this method performs poorly since it always produces over-enhancement and loses details in the areas, where histograms are densely distributed. On the basis of the model of image illumination and reflection components, homomorphic filtering is an approach of image restoration by combining the grey transformation and frequency-domain filtering. This method is skilled at improving the contrast of low-illumination images, whereas the result of restoration looks slightly dark [19]. The WT is also well applied to noise reduction which helps to get clean images such as the wavelet combines morphology or partial differential equations to achieve denoising [20]. In addition, the wavelet algorithm selects threshold and threshold function to improve performance on restoration [21]. The Retinex algorithm is built on the theory of colour constancy based on the visual representation of human [22, 23]. In recent years, this method has ignited much interest in the field of image restoration, and the improvement of Retinex algorithm mainly focuses on optimising kernel function and weight value in multi-scale Retinex (MSR) algorithm. The purpose is to eliminate the problems of halo, artefact and unnatural enhancement in MSR. These methods involve too many parameters; besides, these parameters are fixed values set by experience, which brings the algorithm some limitations.

Overall, to address these mentioned problems, we conduct many experiments about the restoration of complex illumination images in different scenes with different noises, and the main contributions of our work can be summarised as follows.

Contributions: Unlike most of the existing approaches, considering the effect of the global vision, we propose a new way, the guided adaptive MSR (GAMSR) and improvement BayesShrink threshold filtering (IBTF), which is based on double-density dual-tree complex WT (DDDTCWT) domain. This novel algorithm completes the restoration of images with noise and complex illumination and obtains state-of-the-art performance by extensive experiments.

The main contributions of this paper are three-fold:

i.   We introduce the DDDTCWT to image restoration, and then original images are decomposed into high-frequency subband and low-frequency subband. It makes a great performance to restore the images polluted by noise and reduce the impact of complex illumination.

ii. We propose the GAMSR for low-frequency subband from DDDTCWT. Our GAMSR replaces the Gaussian function with guided filtering and devises the adaptive weight coefficient, which avoids selecting the unreliable coefficient by experience. Solely due to this design, could our method achieve the images with a clear edge and more details.

iii. We present the IBTF to deal with high-frequency subband. Taking the advantages of soft threshold and hard threshold into consideration, we innovatively develop a new hierarchical threshold to IBTF. It has achieved a great success in denoising, especially on the occasion where the noise decreased exponentially with the increasing decomposition layers.

2 Related work

In this section, we briefly review previous works related to our method and clarify the difference between them. Specifically, we present related studies from two aspects: (i) Retinex transformation and (ii) wavelet threshold denoising.

2.1 Retinex transformation

Existing Retinex restoration approaches are usually based on traditional algorithms which were put forward by Land in 1971 [24]. The initial theory uses original image $I(x, y)$ and in density image $R(x, y)$ estimated by some methods as the input of the Retinex.

It aims at recovering the latent clean image $R(x, y)$ from its degraded observation $I(x, y)$, which may be produced by noise contamination and complicated illumination introduced during the image acquisition.

The estimation of $L(x, y)$ is key to Retinex processing and has been extensively studied in primal research. For example, Land et al. [25] proposed to select a pathway randomly among N pathways to obtain $L(x, y)$ [25]. McCann and Frankle et al. designed a spiral section comparison path, which selects a path from different random paths [26]. The standard centre/surround Retinex algorithm [27] was to extend the estimation $L(x, y)$ by McCann et al. When studying the Gaussian winding path, Jobson et al. [28] present single-scale Retinex (SSR) and MSR algorithms. The SSR chooses sole scale parameter σ, which cannot obtain enhancement of details and colour fidelity simultaneously and the MSR introduces the small, middle and big scale parameters into restoration, which

solve the SSR problem perfectly. A Retinex algorithm based on bilateral filtering and mean shift filtering is becoming a hot topic recently [29]. The function of bilateral filtering is denoising and retaining edge information filtering. Synthesising of pixels light and location, Hu et al. [30] introducing bilateral filtering into eliminating the halo. Zhou et al. [31] utilised that the mean shift filtering adopts the kernel density estimation to restore image colour.

These works exist some defects such as halo artefacts, multiple iterations and gradient inversion in Gaussian, mean shift and bilateral filtering [32]. Complementary to the above works on image restoration, we conduct a dedicated study on filtering selection and accordingly come up with two solutions that address the crucial issues existed in image restoration. We propose a guide filtering to maintain the image boundary and texture feature to obtain image $L(x, y)$ [33]. In addition, we design an adaptive weight coefficient that effectively optimises the result of image brightness and contrast restoration, which is another major challenge for this task [34].

2.2 Wavelet threshold denoising

The basic methods of wavelet denoising consist of modulus maxima denoising, wavelet coefficient correlation denoising, wavelet threshold denoising and so on. Moreover, the most famous method is the wavelet threshold denoising because of its simple realisation and a small amount of calculation [15, 35, 36]. We will analyse some representative methods for wavelet threshold denoising from threshold processing function and selection of threshold [37].

For threshold processing function, the hard threshold is easy to appear the pseudo-Gibbs effects and while the wavelet coefficient is larger than the threshold, soft threshold wavelet comes out a constant deviation [38, 39]. To improve the inherent defects of soft and hard threshold methods, Gao and Bruce [40, 41] jointly proposed a semi-soft threshold function and the Minimax threshold processing method. However, this method is computationally complicated and is not good at the smoothness of the restored image. Then, Garrotte threshold processing function was put forward in [42]. The threshold function is continuous at the threshold, but its recovery image still has defects of poor smoothness. The threshold function described in this paper not only has a good pro-approximation in the hard threshold function, but also has the advantage of continuity of the soft threshold function.

For a selection of threshold, one famous benchmark is VisuShrink. It is the first proposed threshold estimation function by Donoho and Johnstone [43]. Although its actual application effect
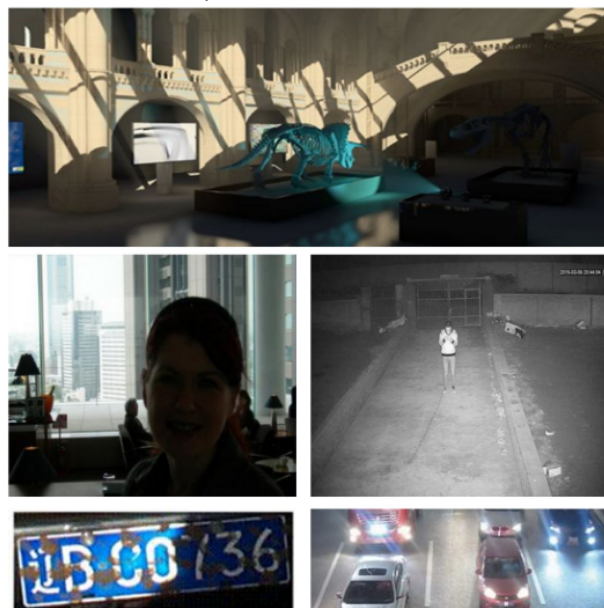

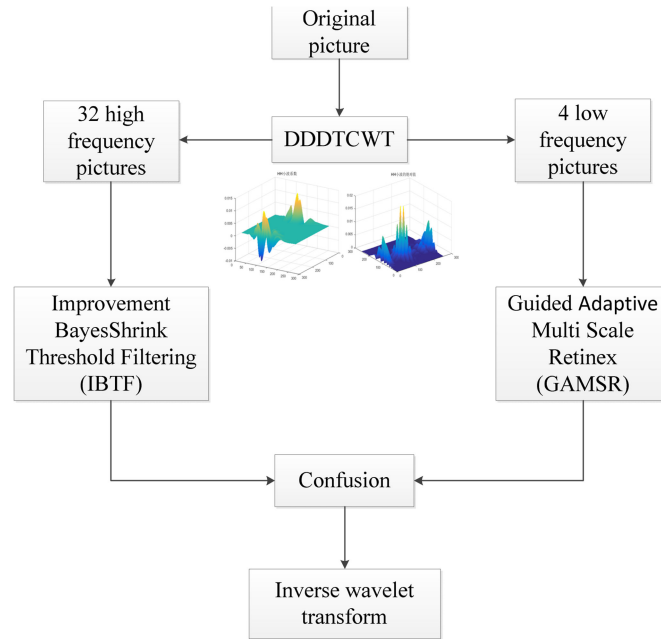**Fig. 1** *Common complex illumination scenes*

Fig. 2 *Algorithm flowchart*

is not good, it triggers more attention to the threshold. The threshold obtained by the SUREShrink method is close to the ideal value [44], but it is computationally complex and many noises cannot be filtered out. Resembling SUREShrink method, BayesShrink [45]. Threshold estimation reduces many deviations so that it is more effective and less computational. In our work, we build a hierachy threshold estimation formula for image restoration to solve the problem that the Bayesian threshold estimation only reaches a global optimum and cannot achieve local optimums.

3 Complex illumination image restoration algorithm based on DDDTCWT

Discrete wavelet transformation (DWT) with multi-resolution becomes a powerful multi-scale analysis tool, due to its ease of implementation and low complexity [46]. However, there are some drawbacks in two-dimensional DWT such as poor directional selectivity, lacking translation invariance, vulnerability to data and easy to appear artefact in the analysis of image under complicated illumination condition. These papers develop a fusion technology base on DDDTCWT to reinforce images captured under complicated illumination condition. Taking the causes of complicated illumination and characteristics of the image with noisy contamination into account, this paper presents IBTF and GAMSR methods to process the decomposed low frequency and high frequency of images by DDDTCWT. At the same time, we also establish a series of objective and subjective criterion systems to evaluate our approach.

3.1 Algorithm description

Our research adapts the DDDTCWT, which decomposes the original image into 4 low-frequency subbands and 32 high-frequency subbands. The main power of image distributes on the low-frequency subbands, which are the similarity and average of the original image. The high-frequency subbands represent the details of the image such as the edge, outline and noise. Since each of subband coefficients has different physical significances, we need to adapt the different methods to restore the low-frequency and high-frequency subbands. During restoring the high-frequency subbands, we focus on the elimination of noise and retention edges etc. The theoretical basis of DDDTCWT is that heavy and small absolute amplitude of the wavelet coefficients were caused by signal and noise. If adapted suitable elimination noise model, we can eliminate small noise coefficients. During the low-frequency subbands, we concentrate on the impact from the complex light.

The optimising Retinex algorithm is applied to minimise the effects of complex lighting. The algorithm is given as follows (see Fig. 2):

i.   Obtain image I for recovery.
ii. Adapt DDDTCWT to image I, get the four low-frequency pictures I_a, I_b, I_c, I_d and 32 high-frequency pictures I_1, I_2, …, I_i, i from 1 to 32.
iii. Use the IBTF to the 32 high-frequency pictures and get the 32 pictures I'_1, I'_2, I'_3, …, I'_i, i from 1 to 32.
iv. Use the GAMSR to the four low-frequency pictures and get four pictures I'_a, I'_b, I'_c, I'_d.
v.   Use the inverse WT to the result of pictures, get the final enhanced image.
vi. Evaluate the final picture.

4 Restore the high-frequency subbands

4.1 Improved threshold processing function

According to the thought of Garrotte threshold processing and combining with the advantages and disadvantages of the soft threshold, we propose the following threshold functions:

$$f(x,\,y) = \begin{cases} i(x,\,y) - T + T \times \dfrac{1 - e^{T - i(x,\,y)}}{1 + e^{T - i(x,\,y)}} & i(x,\,y) > T \\[2ex] 0 & |i(x,\,y)| \le T \\[2ex] i(x,\,y) + T - T \times \dfrac{1 - e^{T + i(x,\,y)}}{1 + e^{T + i(x,\,y)}} & i(x,\,y) < -T \end{cases} \quad (1)$$

We introduce soft and hard thresholds into (1), whose merits contain continuity of a function, asymptote to $f(x,\,y) = i(x,\,y)$ and any higher-order derivative differentiable. Owing to the function continuous at the threshold, it overcomes the drawback that the traditional hard threshold function is prone to turbulence and pseudo-Gibbs effect. In asymptote $f(x,\,y) = i(x,\,y)$ selection, we find that when the wavelet coefficient increases, the $f(x,\,y)$ gain on the wavelet coefficients, which overcome the problem of constant deviations in traditional soft threshold functions. At the same time, any higher-order derivatives can be differential, making the function easier to implement more complex operations.

As shown in Fig. 3, the red, blue and green parts are the result of the algorithm we proposed, hard threshold and soft threshold. We can find that our proposed threshold function performance is close to the soft threshold when the absolute value of wavelet

coefficient is less than the threshold value and it is close to the hard threshold when it is over the threshold. However, there is a gentle change when absolute value reduces to the threshold, which is superior to the hard threshold method. It is the threshold transition zone that enables the new threshold function is more similar to the natural signal function. That is why the threshold function described in this paper has the advantage of the hard and soft threshold functions.

4.2 Bayesian threshold estimation and modification

After many original images and noisy images decomposed by a wavelet, their wavelet coefficients approximately obey Gaussian or Laplace distribution, which is named general Gaussian distributions

$$GG_{\beta, \sigma_x}(x) = C(\beta, \sigma_x)e^{-(\alpha(\beta, \sigma_x)|x|)\beta} \qquad (2)$$

The standard deviation estimation formula of generalised Gaussian distribution is given by Grace Chang *et al.*

$$\sigma_x^2 = \frac{1}{N_j} \sum \omega_j(x, y)^2 \qquad (3)$$

where σ_x^2 is the standard deviation, $\omega_j(x, y)$ represents the number of high-frequency coefficients in the wavelet coefficients and N_j is the corresponding subband wavelet coefficient values.

σ_n^2 represents the variance of the noise. If we cannot predict the noise of the image in advance, we will adapt the method named median estimator to estimate the noise. The median estimate is defined as follows:

$$\sigma_n = \frac{\text{median}(|i(x, y)|)}{0.6745}, \quad i(x, y) \in HH_j \qquad (4)$$

where $i(x, y)$ denotes bandpass coefficient in high-frequency land HH_j.

We define σ_β as the variance estimation of the source image, and it is calculated as follows:

$$\sigma_\beta = \sqrt{\max\left(\sigma_x^2 - \sigma_n^2, 0\right)} \qquad (5)$$

The Bayesian threshold calculating formula is given by

$$T = \begin{cases} \dfrac{\sigma_n^2}{\sigma_\beta} & \sigma_\beta \neq 0 \\ \max\left(|i(x, y)|\right) & \sigma_\beta = 0 \end{cases} \qquad (6)$$

where T is a Bayesian threshold. Bayesian threshold estimation reduces a lot of errors. It is pointed out in the literature [47] that the estimated error of the Bayesian threshold is within 5%, why it has been widely applied.

Since the estimation of Bayesian threshold has been satisfactory, we improve the performance from other aspects. The global thresholds are used to the conventional Bayesian threshold approach. Although the calculation of the global threshold is easy, it just satisfies the global optimal and cannot achieve local optimal. For example, because the first-layer wavelet decomposition coefficient is usually very small, the result of Bayesian threshold estimation will be small. However, the second wavelet is not such as that. That is why this global threshold cannot meet the needs of wavelet decomposition, from which we will improve the algorithm performance.

In our method, the improvement of the algorithm is mainly based on the average modulus of noise and the average modulus maxima according to the index rules attenuation characteristics with the increase of decomposition layers. Contrasting to the noises decreasing rapidly as the number of decomposition layers increase, the image signal will not be decreased significantly. Therefore, we propose a hierarchical threshold estimation formula as follows:

$$T_{AB} = e^{(s - L/2/L)}T_B \qquad (7)$$

where L is the largest scale of wavelet denoising, s represents current decomposition scale and T_B indicates the Bayesian threshold estimation result.

5 Restore the low-frequency subbands

5.1 Guided AMSR

As processing the low-frequency subbands, we introduce guided filtering into the MSR algorithm, which greatly improves the MSR performance with guided filtering's ability to retain edge information.

The guidance filter is a partial multi-point filter, which benefits to maintain the detail. Using the box filters, we define the degree of guided filtering by customising ε. It is necessary to introduce guided images before the image edge is preserved. The guided images usually are taken themselves or take the feature image-by-image segmentation and feature extraction [48]. The grey-scale value of the ith pixel of the bootstrap image is denoted as

$$q_i = \sum_j \omega_{ij}(I)p_j \qquad (8)$$

where I presents guided image, p is the input image, q is the output image, i and j indicate pixel coordinates and ω_{ij} is the filter core.

We suppose that the guided image I and the output image q are linearly dependent and q is a linear transformation relationship with I in a small window ω_k, in which k is the centre. Therefore, the formula is defined as

$$q_i = a_k I_i + b_k, \quad \forall i \in \omega_k \qquad (9)$$

where a_k and b_k are linear coefficients supposed to the constant. This local linear model guarantees that when q is the edge, I is also the edge because of the linear gradients. This model has been proven effectively in many applications.

To confirm the values of a_k and b_k, we define a minimised cost function, which makes the difference value between input and output image minimal. The definition of minimised cost function is as follows:

$$E(a_k, b_k) = \sum_{i \in \omega_k} \left((a_k I_i + b_k - p_i)^2 + \varepsilon a_k^2\right) \qquad (10)$$

where ε is a regularisation parameter between 0 and 1 to prevent the result of a_k too big. The bigger ε is, the heavier smooth multiples superposition is. The above results are obtained by linear regression defined as follows:

$$a_k = \frac{(1/(|\omega|))\sum_{i \in \omega_k} I_i p_i - u_k \bar{p}_k}{\sigma_k^2 + \varepsilon} \qquad (11)$$

where $|w|$ is the number of pixels in the window ω_k, u_k and σ_k^2 are the mean value and the variance of I in the window ω_k and $\bar{p}_k$ is the mean value of P in the window ω_k

$$b_k = \bar{p}_k - a_k u_k \qquad (12)$$

$$q_i = \frac{1}{|w|}\sum_{k, i \in \omega_i} (a_k I_i + b_k) = \bar{a}_k I_i + \bar{b}_k \qquad (13)$$

$$\bar{a}_i = \frac{1}{|\omega|}\sum_{k \in \omega_j} a_k \qquad (14)$$

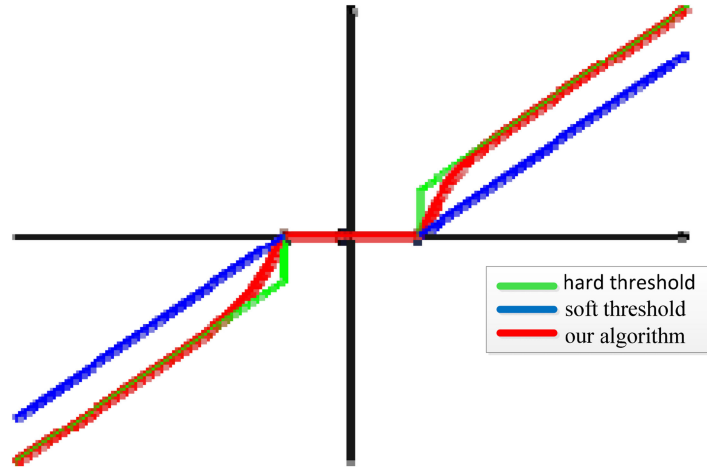$$\bar{b}_i = \frac{1}{|\omega|}\sum_{k \in \omega_j} b_k \qquad (15)$$

Fig. 3 *Paper's threshold function (best viewed online in colour)*

Having adapted the first-order gradient calculation on both sides at the same time, we conclude the formula $\nabla q_i = \bar{a}_i \nabla I_i$, which satisfies the need of linear relation. Therefore, guided filtering has very good edge maintaining characteristics. Meanwhile, a_k determines the degree of maintaining the edge of the image. The smaller a_k is, the more degraded and smoother image edge is.

On the basis of the above theoretical basis, we conclude that ε and a_k used in guiding filtering determine the output image ability which can keep the edge of image complete and smooth. During the transform of Retinex, we used the guiding image instead of a Gaussian function to make the convolution to get the final result which is estimated illumination information.

5.2 Formula of weight coefficient calculation

In the classical MSR algorithm, the selection of coefficient usually depends on experience, which is also the global coefficient. Whether the selection of coefficient is suitable or not determines the brightness and contrast of the restoration image. A number of reference coefficients given by many documents float up and down around 0.3, which has different recovery effects to the different image. To raise the objective weight coefficient, we do the following work.

Assuming that the original image is divided into N blocks, we define H_i as the local entropy for images of the ith block and define Q as the mean entropy for the image. The calculation formula of Q is as follows:

$$Q = \left(\frac{1}{N}\sum_{i=1}^{N}H_i\right)/8 \qquad (16)$$

The calculation formula of the local contrast is as follows:

$$P = 1 - \frac{1}{\bar{m}}\sqrt{\frac{1}{N}\sum_{i-1}^{N}(m_i - \bar{m})^2} \qquad (17)$$

where m_i is the average grey scale for the image of the ith block and $\bar{m}$ is the average grey scale of the whole image.

The calculation formula of the weight coefficient is as follows:

$$p_1 = (P + Q + 1)/3 \qquad (18)$$

$$p_2 = (1 - w_1) \times 2/3 \qquad (19)$$

$$p_3 = (1 - w_1)/3 \qquad (20)$$

We combine the calculation formula of weight coefficient with GAMSR, which is the main algorithm to solve the complex image in this paper.

6 Experiment

6.1 Different methods of image recovery

To verify the real recovery ability of our method in the noisy image restoration, it is compared with the improved histogram equalisation method in [49] and the homomorphic filtering method, Retinex enhancement algorithm based on bilateral filtering [30] and the literature [25] based on WT enhancement algorithm by comparative experiments.

The experiment uses MATLAB 2015b in the Win 7 platform for testing. The scale coefficients of the MSR are set to 20, 80 and 180. The first is recovery denoising experiment. We choose noise-containing pictures to test image recovery ability with the above methods.

In this section, three types of images are selected. The first type is a low-contrast resistance strain gage image. From Fig. 4*a*, it can be seen that the strain gage image to be restored has low contrast, overall whitening and grey points. The primary purpose of image enhancement is to increase the contrast of the strain gage image to highlight the cross-bar details. The results of image restoration are shown in Figs. 4*b–f*. Fig. 4*b* is the enhancement result of homomorphic filtering. Homomorphic filtering solves the problem of overall whitening of the picture. However, it also reduces the brightness of the image, which results in the obscure of the horizontal grid area of the image. The method in [49] is shown in Fig. 4*c*. Although the improved histogram method in [49] greatly improves the overall contrast of the image, it enlarges the grey speckles of the image and causes great disturbance for the image recognition. Fig. 4*d* shows the Retinex transformation algorithm based on double-sideband filtering in [30]. As shown in Fig. 4*d*, the result has higher brightness and contrast, which is clearer in the horizontal bar area. However, Fig. 4*d* does not eliminate the grey spots, and the enhancement of the area around the black triangle above the graph is still not enough. Literature [25] is a traditional wavelet-based image enhancement algorithm. The result of this restoration is slightly better than the method of [49]. On the other hand, the contrast of the enhanced result is still low and has a certain degree of the grey-shift phenomenon. Fig. 4*f* is our recovery algorithm. Intuitively, the method in this paper is more superior than the above methods. The edge of the strain gage image after the restoration of our algorithm is clearer and has better contrast; it also weakens the level of grey spots in Fig. 4*a* and highlights details well.

We evaluate the above results objectively with information entropy H, peak signal-to-noise ratio (PSNR) and sharpness J. The evaluation results are shown in Table 1. To show the recovery results of various methods clearly, we make Table 1 into Fig. 5. It can be seen from Table 1 that the restoration result of homomorphic filtering has limited improvement to PSNR and sharpness. We can see from the recovery pictures that the PSNRs of literatures [49, 25] are not much different, but the information entropy varies greatly, which also points out the limitation of the objective evaluation of the image (see Fig. 6).
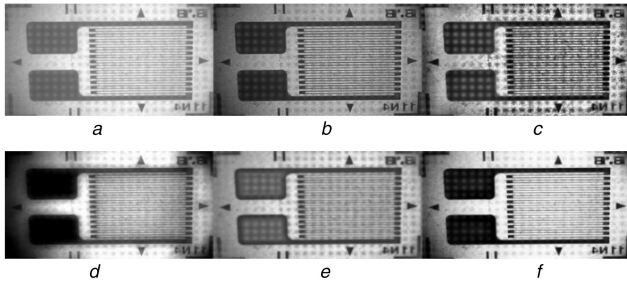
Fig. 4 *Recovery results of resistance strain gauges with different methods*
(a) Original drawing, *(b)* Homomorphic filtering, *(c)* [49], *(d)* [30], *(e)* [25], *(f)* Our algorithm

Table 1 Recovery results of resistance strain gauges

	PSNR	J	H
original drawing	—	1.085	6.869
homomorphic filtering	12.186	1.078	6.5612
[49]	17.551	1.780	7.910
[30]	19.429	2.318	7.522
[25]	15.976	2.050	6.961
our algorithm	23.732	2.941	7.573

Fig. 5 *Objective evaluation results of normalised resistance strain gauges*
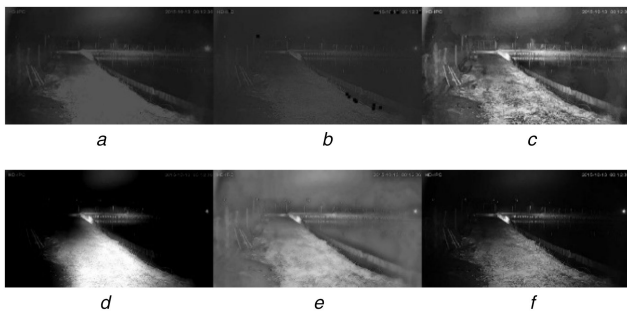

Fig. 6 *Recovery of night surveillance images with different methods*
(a) Original drawing, *(b)* Homomorphic filtering, *(c)* [49], *(d)* [30], *(e)* [25], *(f)* Our algorithm

The recovery method in this paper provides the best PSNR and sharpness. From various evaluation indexes, our algorithm has very good enhancement ability for low-contrast images.

The second category is the image with low overall illumination. We adopt the night image captured by a surveillance camera. Owing to the lack of illumination, the entire image is black and it is difficult to distinguish the characteristics of the image. Fig. 6*b* shows the result of homomorphic filtering. Since the illumination of the original picture is low, the homomorphic filtered picture is more blackish, which is not even as good as the original picture. Literature [49] has a better ability to recover this type of image, but there is an unnatural increase in the image and a slight halo on the road and sky. The details of the literature [30] are relatively clear, but one part is brighter and clearly enhanced. The picture processed

Table 2 Objective evaluation results of night surveillance images with different methods

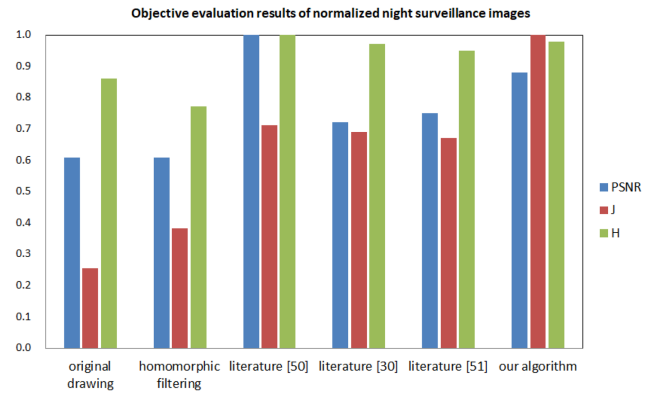|	PSNR	J	H
original drawing	—	**0.778**	**6.234**
homomorphic filtering	12.971	1.175	5.581
[49]	**21.281**	**2.178**	**7.230**
[30]	15.336	2.113	7.022
[25]	**14.976**	**2.055**	**6.861**
our algorithm	18.731	3.061	7.073

Fig. 7 *Objective evaluation results of normalised night surveillance images*
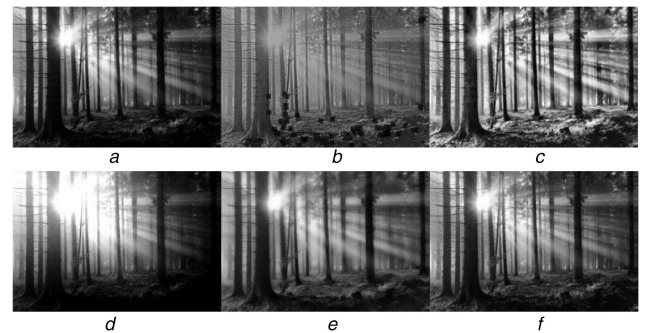

Fig. 8 *Mottled forest images*
(a) Original drawing, *(b)* Homomorphic filtering, *(c)* [49], *(d)* [30], *(e)* [25], *(f)* Our algorithm

with the method of literature [25] is integrally whitening, and the effect of image restoration is moderate. Although after processed with the paper's method, the brightness of the image is slightly low, it can distinguish the texture features on the road surface.

Table 2 is an objective evaluation result of the above pictures. Similar to the above methods, the histogram equalisation method in [49] still has this highest PSNR value. From the objective evaluation histogram of the night surveillance image in Fig. 7, it is clear that our algorithm is only slightly lower than the histogram equalisation method on the PSNR evaluation, and it is ahead of other algorithms on the sharpness *J* evaluation.

The third category is the image of the forest under the shadow. Since the Sun is blocked by trees, the whole image has a distinct alternation of light and shade, which affects the image recognition.

Fig. 8*b* shows the result of homomorphic filtering. Homomorphic filtering emerges black spots near the roots of trees and land, which completely removes mottled sunshine. It makes the picture look very unnatural and have poor readability. The effect of enhancement is very strong with the method in the literature [49]. The trees and the bark part can be seen, but the ground becomes white, which makes contrast too obvious. Although owing to excessive enhancement in the sunlight part, the recovery of sunlight gives a dazzling sensation in the literature [30], the twigs of the trees are still clearly visible. The enhanced image in the literature [25] is not as strong as the literature [30]. Its overall contrast is general, and the trunks in the vicinity can be

Table 3 Objective evaluation results of forest image

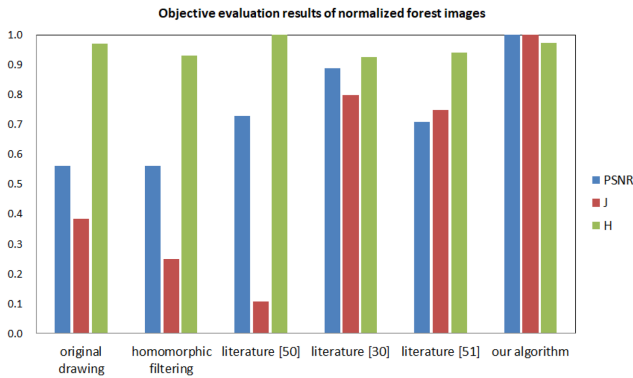|	PSNR	J	H
original drawing	—	**1.787**	**7.672**
homomorphic filtering	14.330	1.166	7.365
[49]	**18.559**	0.498	**7.906**
[30]	22.642	3.730	7.321
[25]	**18.094**	**3.491**	**7.433**
our algorithm	25.508	4.667	7.699

Fig. 9 *Objective evaluation results of normalised forest images*
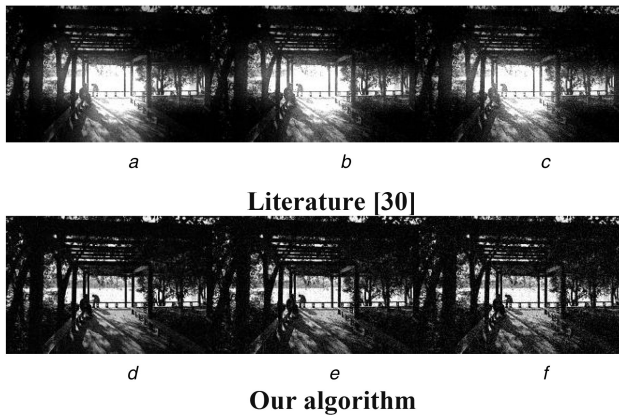

Fig. 10 *Comparison of two restoration algorithms under small noise*
(a) $\sigma = 10$, *(b)*$\sigma = 20$, *(c)*$\sigma = 30$ [30], *(d)* $\sigma = 10$, *(e)* $\sigma = 20$, *(f)* $\sigma = 30$ Our algorithm

clearly distinguished, but the enhancement effect to the distance is poor.

The restored image in this paper is not strong, but it is enough to see the tree's roots and the soil. Table 3 shows the results which are an objective evaluation of restored forest images. Fig. 9 displays the histogram drawn on the basis of Table 3. Since the whole image is much better than the previous, the PSNR and information entropy value after recovery is relatively large. The accuracy is similar after separately restoring in the algorithm proposed in the literature [30], the literature [25] and this paper, but our overall recovery index is still ahead of the above algorithms.

By analysing the experimental recovery results of three common types of complex illumination images, it is found that our algorithm can provide the maximum sharpness and information entropy under the condition of same weak noise. The algorithm proposed in [30] is also superior to traditional homomorphic filtering and the improved histogram equalisation method in the literature [49]. We have proved that the traditional Gaussian Retinex can easily amplify the noise and generate the halo. Therefore, we will use the method in the literature [30] to carry out denoising experiments with our algorithm.

6.2 Algorithm of denoising enhancement experiment

Hu *et al.* [30] pointed out that Retinex based on bilateral band filtering has a good ability to suppress noise. To verify the ability
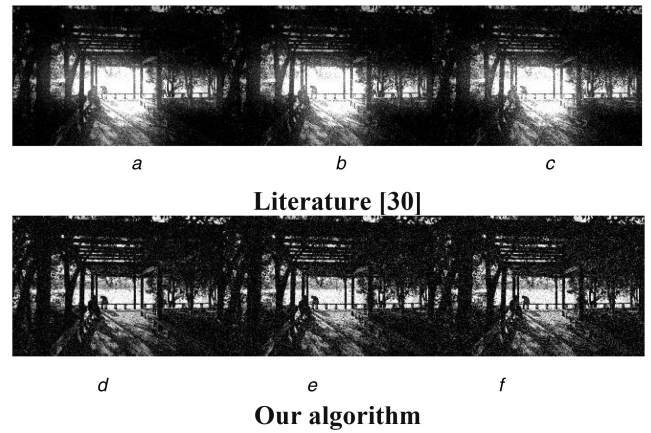

Fig. 11 *Comparison of two restoration algorithms under middle noise*
(a) $\sigma = 40$, *(b)*$\sigma = 50$, *(c)*$\sigma = 60$ [30], *(d)* $\sigma = 40$, *(e)* $\sigma = 50$, *(f)* $\sigma = 60$ Our algorithm
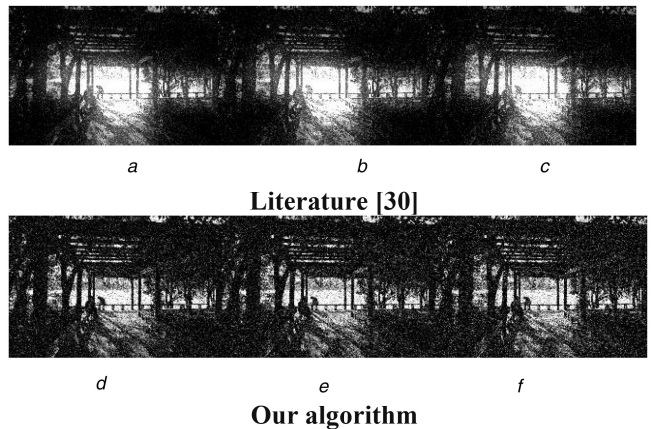

Fig. 12 *Comparison of two restoration algorithms under strong noise*
(a) $\sigma = 70$, *(b)*$\sigma = 80$, *(c)*$\sigma = 90$ [30], *(d)* $\sigma = 70$, *(e)* $\sigma = 80$, *(f)* $\sigma = 90$ Our algorithm

of our algorithm to eliminate different noises, we select the method proposed in the literature [30] to check the test. Gaussian white noisy images with an increasing mean value from 0 to 100 are used. The following are the result images.
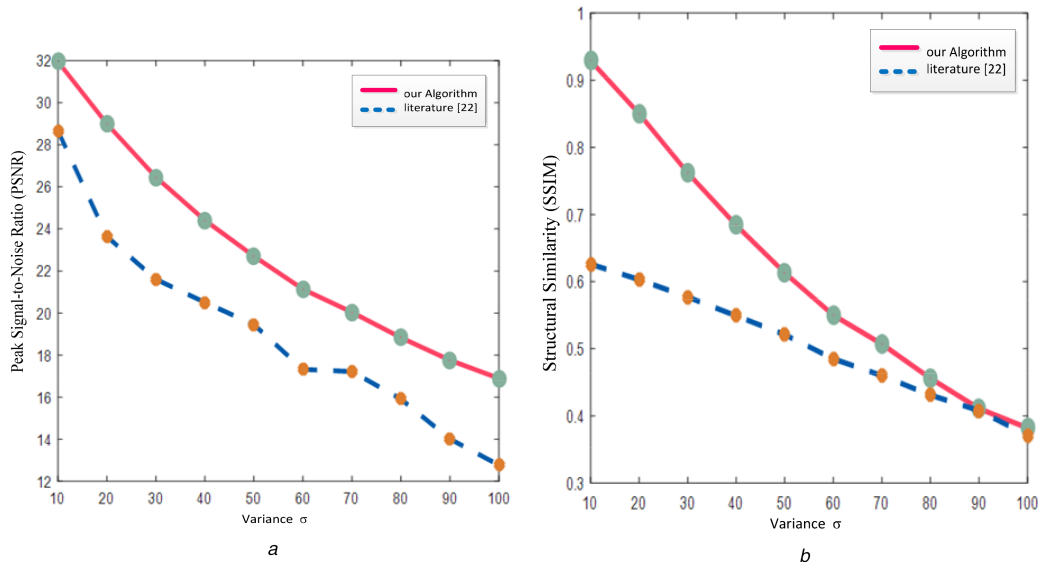
Fig. 10 shows the experimental results under small noise. It can be seen from the figure that the restoration algorithm in the literature [30] is slightly light and bright, and the local contrast in the bright area is not enough, which affects the observation of some details. Although the recovery result of our algorithm is slightly darker, the restoration is more natural.

In Fig. 11, the Gaussian noise variance is between 40 and 60. From recovery results, the results which are processed separately with these algorithms appear to amplify the noise partially in such a noise case. However, the result of our algorithm has less noise.

Fig. 12 is the restored image under strong noise interference. The variance of noise is between 70 and 90. The quality of the recovery results is degraded by both methods. However, our algorithm is still superior to the literature [30]. As can be seen from Table 4, both the PSNR and the structural similarity (SSIM) values of two algorithms are decreasing while noisy variance increases. However, the decrease of our algorithm is less. We take the picture as an example whose mean variance is equal to 50. The value of PSNR result gotten by our algorithm is 22.7, whereas it dropped to 19.4 when the picture is processed by the method proposed in the literature [30]. Moreover, the value of mean squared error (MSE) also clearly shows the difference between the two methods. The smaller the value of MSE is, the more similar the noise-free recovery result is. The method proposed in this paper can basically filter out most of the Gaussian noise when the noise variance is <50. Since the method of noise suppression is used in the literature [30], the MSE value of a recovered picture is larger. The sharpness of the two methods has a considerable difference. Therefore, our algorithm is obviously superior to the method in the literature [30].

Table 4 Recovery results of two recovery algorithms under different noise conditions

	Variance	10	20	30	50	60	80	90	100
PSNR	[30]	**28.659**	**23.632**	**21.603**	**19.449**	**17.320**	**15.910**	**14.014**	**12.769**
	our algorithm	31.950	28.990	26.456	22.704	21.134	18.830	17.757	16.893
MSE	[30]	**0.023**	**0.032**	**0.044**	**0.049**	**0.507**	**0.549**	**0.580**	**0.653**
	our algorithm	0.001	0.001	0.002	0.005	0.008	0.013	0.017	0.021
SSIM	[30]	**0.626**	**0.603**	**0.577**	**0.521**	**0.485**	**0.431**	**0.408**	**0.371**
	our algorithm	0.929	0.850	0.762	0.613	0.550	0.456	0.411	0.382
J	[30]	**2.85**	**2.65**	**2.41**	**1.87**	**1.60**	**1.19**	**1.04**	**0.90**
	our algorithm	5.46	5.01	4.56	3.40	2.94	02.20	2.00	1.75
H	[30]	**6.123**	**6.144**	**6.134**	**6.117**	**6.095**	**6.065**	**6.048**	**6.014**
	our algorithm	6.580	6.601	6.578	6.565	6.610	6.550	6.516	6.548

Fig. 13 *Objective evaluation variation diagram (best viewed online in colour)*
(a) PSNR, *(b)* SSIM

To show the difference between the two methods in PSNR and SSIM intuitively, the graphs of SSIM and PSNR variation with noise variance has been plotted according to the aforementioned data. As shown in Fig. 13, the red line is our algorithm and the blue line is literature [30]. It can be seen clearly from these pictures that our algorithm changes smoother with the increase of noise. The algorithm mentioned in the literature [30] is not only easy to be influenced by noise, but also numerically fluctuated greatly.

7 Conclusions

In this paper, a restoration algorithm of images with noise and complex illumination is proposed, which involves DDDTCWT and MSR transform. This algorithm first decomposes the original images into low-frequency subbands and high-frequency subbands with DDDTCWT. Then, the illumination is mainly distributed in low-frequency subbands and the noise is mainly distributed in high-frequency subbands. We exploit improved MSR transform and Bayesian denoising methods to deal with two kinds of subbands, which make high-frequency subbands denoised and preserve the edge and low-frequency subbands minimise the illumination complexity. Finally, the restored images come out after utilising inverse WT. The experimental results show that the proposed method can effectively optimise the details, edges and textures of the complex illumination images, it can also reduce the noise and improve the contrast [33].

8 Acknowledgment

9 References

[1] Gianini, G., Rizzi, A., Damiani, E.: 'A Retinex model based on absorbing Markov chains', *Inf. Sci.*, 2016, **327**, pp. 149–174
[2] Zhang, Y., Zhang, F., Li, B.: 'Image restoration method based on fractional variable order differential', *Multidimens. Syst. Signal Process.*, 2018, **29**, pp. 999–1024
[3] Wang, Q., Gao, J., Yuan, Y.: 'A joint convolutional neural networks and context transfer for street scenes labeling', *IEEE Trans. Intell. Transp. Syst. (T-ITS)*, 2018, **19**, (5), pp. 1457–1470
[4] Zhang, Y., Sun, L., Yan, C*., et al.*: 'Adaptive residual networks for high-quality image restoration', *IEEE Trans. Image Process.*, 2018, **PP**, (99), p. 1
[5] Mei, S., Ji, J., Hou, J*., et al.*: 'Learning sensor-specific spatial-spectral features of hyperspectral images via convolutional neural networks', *IEEE Trans. Geosci. Remote Sens.*, 2017, **55**, (8), pp. 4520–4533
[6] Wang, N., Qi, L., Dong, J*., et al.*: 'Two-stage underwater image restoration based on a physical model'. Eighth Int. Conf. Graphic & Image Processing, Tokyo, Japan, 2017, p. 10225
[7] Fau, M., Hassan, A., Shahrizan, A*., et al.*: 'Enhancement of under-exposed image for object tracking algorithm through homomorphic filtering and mean histogram matching'. Int. Conf. Computational Science & Engineers, Paris, France, 2016
[8] Li, Q., Xu, F., Zhao, X*., et al.*: 'High resolution image restoration algorithm of wavefront coding system based on wiener filter and wavelet de-noising', *Optoelectron. Imaging Multimedia Technol. IV*, 2016, **10020**, p. 1002018
[9] Mei, S., Bi, Q., Ji, J*., et al.*: 'Hyperspectral image classification by exploring a low-rank property in spectral or/and spatial domain', *IEEE J. Sel. Top. Appl. Earth Obs. Remote Sens.*, 2017, **10**, (6), pp. 2910–2921
[10] Qiao, N.: 'An improved histogram equalization', *Opt. Technol.*, 2008, **34**, (S1), pp. 141–142
[11] Zhang, Y., Wu, L., Li, T*., et al.*: 'Enhancement of image histogram equalization based on PCNN', *J. Southeast Univ. (Nat. Sci.)*, 2010, **40**, (01), pp. 64–68

[12] Wen, H., Qi, W., Shuang, L., *et al.*: 'Medical X-ray image enhancement based on wavelet domain homomorphic filtering and CLAHE'. 2016 Int. Conf. Robots & Intelligent System (ICRIS), Zhangjiajie, Hunan Province, 2016, pp. 249–254

[13] Li, J., Lu, C., Zhang, F., *et al.*: 'Contrast enhancement for images of raised characters on region of interest', *Intell. Control Autom. IEEE Xplore*, 2010, pp. 6258–6261

[14] Vishwakarma, A., Mishra, A., Gaurav, K., *et al.*: 'Illumination reduction for low contrast color image enhancement with homomorphic filtering technique'. Int. Conf. Communication Systems and Network Technologies IEEE, Rajkot, India, 2012, pp. 171–173

[15] Shalchian, B., Rajabi, H., Soltanian-Zadeh, H.: 'Assessment of the wavelet transform in reduction of noise from simulated PET images', *J. Nucl. Med. Technol.*, 2009, **37**, (4), p. 223

[16] He, Y., Liu, C., Xu, Z., *et al.*: 'Joint wavelet denoising of vehicle braking signals based on a soft threshold and genetic adaptive threshold', *Veh. Eng.*, 2014, **36**, (06), pp. 703–708

[17] Banic, N., Loncaric, S.: 'Light random sprays Retinex: 'exploiting the noisy illumination estimation', *IEEE Signal Process. Lett.*, 2013, **20**, (12), pp. 1240–1243

[18] Fan, C., Chen, J., Liang, C., *et al.*: 'Accelerating multi-scale Retinex using ARM NEON'. IEEE Int. Conf. Consumer Electronics – Taiwan IEEE, Hong Kong, 2014, pp. 77–78

[19] Gao, T., Zhao, X., Chen, T., *et al.*: 'Illumination-insensitive image representation via synergistic weighted center-surround receptive field model and Weber law', *Pattern Recognit.*, 2017, **69**, pp. 124–140

[20] Wang, Q., Gao, J., Yuan, Y.: 'Embedding structured contour and location prior in siamesed fully convolutional networks for road detection', *IEEE Trans. Intell. Transp. Syst. (T-ITS)*, 2018, **19**, (1), pp. 230–241

[21] Lu, H., Li, S., Liu, Q., *et al.*: 'MF-LRTC: 'multi-filters guided low-rank tensor coding for image restoration'. IEEE International Conference on Image Processing, IEEE, 2017, pp. 2104–2108

[22] Hussain, M., Akbari, A.: 'Color constancy algorithm for mixed-illuminant scene images', *IEEE Access.*, 2018, **6**, pp. 8964–8976

[23] Mei, S., Hou, J., Chen, J., *et al.*: 'Simultaneous spatial and spectral low-rank representation of hyperspectral images for classification', *IEEE Trans. Geosci. Remote Sens.*, 2017, doi: 10.1109/TGRS.2017.2785359

[24] Land, E., McCann, J.: 'Lightness and Retinex theory', *J. Opt. Soc. Am.*, 1971, **61**, (1), pp. 1–11

[25] Shengdong, P., Xiangjing, A., Hongtao, X., *et al.*: 'Improving iterative Retinex algorithm for dynamic range compression', *Adv. Mater. Res.*, 2013, pp. 756–759, 2892-7

[26] Land, E., Mccann, J.: 'Lightness and retinex theory', *J Opt Soc Am*, 1971, **61**, (1), pp. 1–11

[27] Land, E.: 'Recent advances in Retinex theory', *Vis. Res.*, 1986, **26**, (1), p. 7

[28] Jobson, D., Rahman, Z., Woodell, G., *et al.*: 'Properties and performance of a center/surround retinex', *IEEE Trans. Image Process.*, 1997, **6**, (3), pp. 451–462

[29] Wang, Q., Wan, J., Yuan, Y.: 'Locality constraint distance metric learning for traffic congestion detection', *Pattern Recogn. (PR)*, 2018, **75**, pp. 272–281

[30] Hu, W., Wang, R., Fang, S., *et al.*: 'Retinex algorithm for image enhancement based on bilateral filtering', *J. Eng. Graph.*, 2010, **31**, (2), pp. 104–109

[31] Zhou, Y., Sun, J., Niu, B.: 'Retinex-based color image enhancement algorithm by improved mean shift filtering', *Comput. Sci.*, 2014-S1

[32] Mei, S., Yuan, X., Ji, J., *et al.*: 'Hyperspectral image spatial super-resolution via 3D full convolutional neural network', *Remote Sens.*, 2017, **9**, (11), p. 1139

[33] Gao, T., Zhao, X., Xiang, M., *et al.*: 'Texture feature descriptor using auto salient feature selection for scale-adaptive improved local difference binary', *Multidimens. Syst. Signal Process.*, 2017, **28**, (1), pp. 1–12

[34] Gao, T., Zhao, X., Chen, T., *et al.*: 'Face description based on adaptive local weighted Gabor comprehensive histogram feature', *Multimedia Tools Appl.*, 2017, **76**, (10), pp. 1–24

[35] Li, L., Liu, J., Wang, J.: 'Research on image denoising based on wavelet adaptive threshold', *Electron. Technol. (UK)*, 2017

[36] Xue, T., Li, X., Chen, Y.: 'A double threshold wavelet de-noising method for gas liquid bubble flow under high speed photography', *J. Optoelectron. laser*, 2016, **27**, (02), pp. 217–223

[37] He, Y., Liu, C., Xu, Z.: 'Combined Wavelet Denoising for Vehicle Braking Noise Signal Based on Both Soft Threshold and Genetic Algorithm-based Adaptive Threshold', *Automot. Eng.*, 2014, **36**, (06), pp. 703–708

[38] Zhong, J., Jian, S., You, C., *et al.*: 'Wavelet de-noising method with threshold selection rules based on SNR evaluations', *J. Tsinghua Univ. (Sci. Technol.)*, 2014, **54**, (2), pp. 259–263

[39] Joseph, S., Babu, A.: 'Wavelet energy based voice activity detection and adaptive thresholding for efficient speech coding', *Int. J. Speech Technol.*, 2016, **19**, (3), pp. 537–550

[40] Gao, H., Bruce, A.: '*Waveshrink and Semisoft Shrinkage*' (Statsci Division of Mathsoft Inc., 1995)

[41] Gao, H., Bruce, A.: 'Waveshrink with firm shrinkage', *Stat. Sin.*, 1997, **7**, (4), pp. 855–874

[42] Gao, H.: 'Wavelet shrinkage denoising using the non-negative Garrote', *J. Comput. Graph. Stat.*, 1998, **7**, (4), pp. 469–488

[43] Donoho, D., Johnstone, J.: 'Ideal spatial adaptation by wavelet shrinkage', *Biometrika*, 1994, **81**, (3), pp. 425–455

[44] Wang, Q., Wan, J., Yuan, Y.: 'Deep metric learning for crowdedness regression', *IEEE Trans. Circuits Syst. Video Technol. (T-CSVT)*, 2017, doi: 10.1109/TCSVT.2017.2703920

[45] Starck, J., Candes, E., Donoho, D.: 'The curvelet transform for image denoising', *IEEE Trans. Image Process.*, 2002, **11**, (6), pp. 670–684

[46] Guo, X., Zhang, D., Xue, H., *et al.*: 'All attitude north-seeking based on wavelet de-noising and TLS algorithm', *Syst. Eng. Electron. Technol.*, 2016, (02), pp. 362–367

[47] Robinson, M., McCarthy, D., Smyth, G.: 'Edger: a bioconductor package for differential expression analysis of digital gene expression data', *Bioinformatics*, 2010, **26**, (1), pp. 139–140

[48] Gao, T., Zhao, X., Chen, T., *et al.*: 'Image feature representation with orthogonal symmetric local Weber graph structure', *Neurocomputing*, 2017, **240**, (C), pp. 70–83

[49] Chen, W., Liao, B., Xu, X., *et al.*: 'Histogram equalization enhancement for images based on piecewise image enhancement way', *J. Commun.*, 2011, **32**, (09), pp. 153–160